Journal of Energy Storage 77 (2024) 109898

Contents lists available at ScienceDirect

Journal of Energy Storage

journal homepage: www.elsevier.com/locate/est

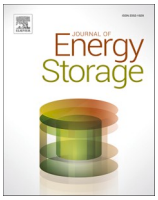

Research papers

Techno-economic assessment and grid impact of Thermally-Integrated Pumped Thermal Energy Storage (TI-PTES) systems coupled with photovoltaic plants for small-scale applications

Luca Migliari *, Mario Petrollese, Giorgio Cau, Daniele Cocco

Department of Mechanical, Chemical and Materials Engineering, University of Cagliari, Via Marengo, 2, 09123 Cagliari, Italy

ARTICLE INFO

Keywords:
Pumped thermal energy storage
Organic Rankine cycle
High temperature heat pump
Thermal energy storage
Heat recovery
Grid security

ABSTRACT

The growing share of Renewable Energy Sources (RES) is rising the amount of curtailed energy to preserve grid security. With the aim of evaluating a complementary storage solution to electric batteries for both new and revamping RES power plants, this study investigates the performance of a Thermally Integrated Pumped Thermal Energy Storage (TI-PTES) system integrated with a Photovoltaic (PV) power plant aimed to enhance the energy self-sufficiency of small-scale users. The assessment is carried out for a case study characterized by a demand of electricity, heating and cooling that vary throughout the year. The studied PTES system is based on the integration of a High Temperature Heat Pump (HTHP), two Thermal Energy Storage (TES) sections and an Organic Rankine Cycle (ORC) power plant. Results show the influence of the main design parameters, such as PV size, HTHP size and TES capacities on the overall system performance, evaluated by means of the energy self-sufficiency, energy self-consumption, round-trip efficiency, Levelized Cost of Storage and the Grid Impact indicator, which quantifies the energy exchanges with the grid (feed-ins and withdrawals) to the overall user demand. The influence of seasonality on the energy performance indicators was studied as well. For the case study considered, the best combination of design parameters for the PV-PTES system is identified with reference to a PV plant whose yearly energy production equals the energy demand and for a 55 kWe High Temperature Heat Pump, a 10 kW ORC and a storage volume of 48 m^3 for each of the two TES units. The PTES system is characterized by a LCOS of 0.72 $/kWh, a round-trip efficiency of 28.2 % and its integration offers several advantages over the use of a PV plant without any storage section. In particular, the PTES unit leads to a substantial increase in the self-sufficiency, within the range 1–14 %, and a considerable decrease of the grid impact indicator, within the range 2–28 %.

1. Introduction

In many countries, the percentage of curtailed wind and solar Photovoltaic (PV) power for grid security reasons is rising along with the growth of Renewable Energy Sources (RES) production [1]. This trend is most notable in areas where grid infrastructure investments and market design and regulation are not in line with the rapid increase in RES development [2]. In Italy, for example, curtailment of wind energy production reached 4.2 % in 2020 [3]. Curtailment of RES generation reduces their economic attractiveness and diminishes the benefits from RES such as environmental advantages, cost-effective electricity, and fuel savings [4].

The grid security can be enhanced, in conjunction with investments and network management strategies, both by providing RES plants with energy storage systems (ESS) [5] and by increasing the number of flexible and agile electricity suppliers [6] able to smooth RES intermittent and variable output profiles [7,8]. In this framework, a promising solution can be found in Pumped Thermal Energy Storage (PTES) [9], a thermo-mechanical energy storage (TMES) technology [10]. With reference to grid-scale medium/long-duration energy storage systems, TMES is a promising alternative to pumped-hydro energy storage (PHES) system, which accounts for over 96 % of the total world energy storage capacity [11]. The major disadvantages of PHES systems are their constraints on location [12] and long construction-process time [13]. TMES systems overcome these disadvantages, keeping, and

* Corresponding author.
E-mail address: luca.migliari@unica.it (L. Migliari).

https://doi.org/10.1016/j.est.2023.109898
Received 9 October 2023; Received in revised form 22 November 2023; Accepted 26 November 2023

Nomenclature

Symbols

c	specific heat [kJ/kgK]
E	energy [kWh]
$\dot{E}$	power [kW]
h	specific enthalpy [kJ/kg]
M	mass [kg]
$\dot{m}$	mass flow rate [kg/s]
$\dot{Q}$	thermal power [kW]
t	time [h]
T	temperature [°C]
V	volume [m^3]
η	efficiency

Subscripts

C	cold
CS	Cooling System
DC	Data Center
G	grid
H	hot
in	inlet side
out	outlet side
U	user
y	year

Acronyms

2T-TES	Two-Tank Thermal Energy Storage
COP	Coefficient Of Performance
CHP	Combined Heat and Power
ESS	Energy Storage System
GI	Grid Impact
HP	Heat Pump
HTHP	High Temperature Heat Pump
HVAC	Heating Ventilation Air Conditioning
HX	Heat Exchanger
LCOS	Levelized Cost of Storage
ORC	Organic Rankine Cycle
PTES	Pumped Thermal Energy Storage
PV	Photovoltaic
RES	Renewable Energy Sources
R-TES	Recovered Thermal Energy Storage
SC	Self Consumption
SS	Self Sufficiency
TES	Thermal Energy Storage
TMES	Thermo-Mechanical Energy Storage

increasing, PHES advantages. In fact, TMES systems have distinctive sector-coupling features, cyclical stability, long lifetimes, low ecological and installation footprints, low specific costs (often under 100 $/kWh), and round-trip efficiencies higher than 60 % [14]. These values are referred to the definition of round-trip efficiency as the ratio of the electric energy output during discharging to the electric energy input during charging and account for the beneficial effects of thermal integration during the charging phase. In addition, TMES systems can supply thermal energy in parallel to electrical energy during discharge, as well as they can receive heat from other energy sources during charge, in the so-called Thermally-Integrated configurations. Differently from conventional cogeneration systems, in TMES the ratio between heat and delivered electricity can be varied depending on thermal demand without heat dissipation. These factors allow TMES systems to be well integrated with many thermal energy-based power generation systems. In particular, in PTES systems the thermal energy is stored at different temperature levels in two reservoirs. Also known as Carnot Batteries, these systems use thermodynamic cycles to convert electricity into heat during charging phases and vice versa during discharging phases. An interesting feature of PTES technology is that it offers a viable approach to enable time shifting of energy in those situations where safety regulations (i.e., fire prevention) impose restrictions on the utilization of conventional Battery Energy Storage Systems (BESS). Furthermore, they do not experience significant capacity degradation over time [15], they do not require critical materials [17], they are characterized by an operating life of more than 30 years [16] and exhibit a reduced environmental impact [18] both during operation (especially if storage media is water) and concerning their end-of-life disposal. Frate et al. [16] described the advantages of TI-PTES over BESS also in terms of OPEX, CO_2 emissions, primary energy consumption and RES curtailment. In fact, due to their ability to store and provide multiple energy vectors [34], TI-PTES are regarded as a key complement of BESS in future scenarios featuring large penetrations of RES [16].

Depending on the thermodynamic cycle, PTES systems can be mainly classified into Joule-Brayton, transcritical (mostly using CO_2 as working fluid) and Compressed Heat Energy Storage (CHEST). The last one uses conventional steam Rankine cycles or Organic Rankine Cycle (ORC) alternatives for the discharging phase and a Heat Pump (HP) for the charging phase: CHEST systems are conceived so that the HP raises the temperature of a storage medium using excess electricity produced by RES and (possibly) waste heat, and the ORC unit converts thermal energy into electricity when needed. Using an ORC-CHEST system also allows to operate at lower temperature and pressure, making possible the use of already commercially available main components (i.e., heat pumps) [19]. It is noteworthy that, at power levels up to 5 MW, systems based on organic working fluids are more efficient than those based on water [14]. Referring to the main performance and cost characteristics of these systems, energy density of transcritical cycles is in the range of 10 ÷ 15 kWh/m^3, Joule-Brayton 20 ÷ 50 kWh/m^3 and CHEST 40 ÷ 100 kWh/m^3. Power densities are in the range of 0.5 ÷ 17 kW/m^3 for CHEST, 2 ÷ 7.5 kW/m^3 for transcritical and 1 ÷ 15 kW/m^3 for Joule-Brayton. Technology Readiness Levels (TRL) vary from 2 to 5 for all cases [10,20–24].

Furthermore, PTES systems can be easily integrated with other energy systems. Several studies involve the waste heat recovery for charging the reservoirs or in manufacturing processes. Other studies concern the integration of PTES systems with PV [25], solar thermal [26], geothermal [27] and Concentrated Photovoltaic (CPV) [17] energy systems. Additional studies regard the re-use of existing parts (i.e., power block) of coal-fired power plants [28], or the inclusion of PTES in some contexts for improving energy independence [29,30]. A comprehensive energy, exergy, and economic analysis of a MW-scale PTES electrically and thermally integrated with a CPV/T plant was carried out by Kurşun et al. [17], which studied a system configuration where the HP electric power derives from PV modules, a CPV/T system and wind turbines, while the HP heat sink is represented by the thermal energy produced by the CPV/T system. Still with reference to TI-PTES systems, Hu et al. [31] studied the influence on the round-trip efficiency and on the Levelized Cost of Storage (LCOS) of design parameters such as the evaporation temperature of HP, the storage temperature (two tanks), the compressor and turbine efficiency and the pinch point temperature differences (HP and ORC).

The design aspects of a small-scale PTES system based on a HP-ORC plant have been studied by Steger et al. [32], who designed a 15 kW HP-ORC system with a storage of water at temperatures of 90–120 °C. With an ORC efficiency of 10.2 % and a HP COP of 5.8, the power-to-power-efficiency (calculated as the ratio of the electrical energy released by the storage and the electrical energy consumed to charge it) of the plant is

59 % and the electrical storage density is 3.6 kWh/ton. Other projects consider higher temperature lifts, albeit at the expense of lower efficiencies. For example, within the CHESTER [33] project a HP with an input power of 4.15 kWe using R-1233zd(E) as the working fluid was designed. With a low temperature heat source of 40 °C, an evaporator temperature of 34.1 °C and a condensation temperature of 134 °C, the COP is around 2.3.

As demonstrated by the cases reported above, several studies on HP-ORC PTES systems have been carried out, with the intention to demonstrate both the technical feasibility and the expected performance of such a system. However, to the authors' knowledge, no study investigates the expected energetic and economic performance of a small-scale HP-ORC PTES configuration in a real operational context, considering daily and seasonal variations in both electrical and thermal energy demand and supply. For this reason, with the aim of meeting this research gap, an advanced energy system configuration, based on a PV power generation plant integrated with a PTES system, is herein modelled and studied. In particular, the energy storage system is based on the coupling between a High Temperature Heat Pump (HTHP), two Thermal Energy Storage (TES) sections and an ORC power unit. Apart from studying a system configuration which includes the recovery and valorisation of low-enthalpy waste heat in a small-scale application, the novelty of this study is the assessment of the seasonal and yearly performance of the proposed PV-PTES for a real energy context and through a new evaluation criterion, herein introduced. A parametric analysis was carried out on the main PV-PTES design parameters, such as PV size, HTHP size and TESs capacities, in order to assess their influence on the system overall performance.

2. Case study

The case study of the present work is represented by the University of Cagliari rectorate energy context, which is characterized by an annual electricity consumption of approximately 0.5 GWh. Out of this total, 28 % is required for powering the data center cooling system ($E_{DC,CS}$), 5 % is dedicated to the Heating, Ventilation, and Air Conditioning system (E_{HVAC}), and the remainder is utilized for the other loads ($E_{RESIDUAL}$). Beside the large share of electricity demanded by the data center cooling system, an important amount of thermal energy produced by the cooling system is released to the environment at a temperature level of about 40–45 °C. More detailed information on yearly energy flows, power ranges and temperature levels can be found in [35], but main data are reported in Table 1. Moreover, Fig. 1 shows the monthly (a) and average daily (b) electricity consumption.

The present study aims to propose an advanced energy supply system for small-scale applications based on the integration of a PV power plant with a PTES system. In particular, Fig. 2 shows the integration of the main components of the proposed PV-PTES system with the current devices (HVAC, DC-CS and Residual) in a simplified diagram. Energy flows are also highlighted. The waste heat generated by the data center cooling system is stored in a single tank Recovered Thermal Energy Storage (R-TES). The R-TES represents a low-temperature source for a HTHP driven by the PV plant. The high-temperature heat produced by the HTHP is stored, during light hours, in a Two-Tank Thermal Energy Storage (2T-TES) system and used, during night hours, by the ORC unit. Brazed plate heat exchangers (HE) are considered for the heat transfer among all system components. To minimize the environmental risks in case of leaks, water is considered as a storage medium for all TES systems.

Table 1
Main characteristics of the case study energy demand.

Overall yearly electricity demand (E_U)	503	MWh
Yearly data center cooling system electricity demand ($E_{DC,CS}$)	141	MWh
Yearly HVAC system electricity demand (E_{HVAC})	23	MWh
Yearly residual electricity demand ($E_{RESIDUAL}$)	338	MWh
Overall electric power demand range	4–153	kW
Data center cooling system electric power demand range	7–30	kW
Data center cooling system thermal power range	31–127	kW
Data center cooling system thermal power temperature range	40–45	°C
HVAC electric power demand range	0–55	kW

The operational logic of the PV-PTES system ensures that the energy generated by the PV plant is first used to meet the electrical loads (HVAC, DC-CS, Residual). If there is any surplus energy, it is used to operate the HTHP, and ultimately, any excess production is fed into the grid. Obviously, the HTHP can only be operated if the R-TES has a sufficient charge level. At the end of the day, or whenever the PV production is zero, the ORC unit can run using the heat stored in the 2T-TES.

3. System modelling

The model of the integrated energy system was developed in MATLAB® [36]. The main features of the different PV-PTES components are described in the following sections.

3.1. Photovoltaic power plant

The PV system power output was calculated starting from the yearly weather data for the site provided by the Meteonorm software [37], with the following equation reported by Petrollese et al. [38]

$$\dot{E}_{PV} = n_{PV} \bullet S_{PV} \bullet GSI \bullet f_{PV} \bullet \eta_{INV} \bullet \eta_{PV} \quad (1)$$

where n_{PV} is the number of PV modules, S_{PV} the module surface, GSI the Global Solar Irradiation, f_{PV} the derating factor for secondary losses, η_{INV} the inverter efficiency (as represented in Fig. 3) and η_{PV} the conversion efficiency of a module, calculated according to Duffie et al. [39] as:

$$\eta_{PV} = \eta_{PV,STC} \bullet [1 + \gamma \bullet (T_{CELL} - 25°C)] \quad (2)$$

where $\eta_{PV,STC}$ is the conversion efficiency at standard test conditions (STC), γ is the temperature coefficient and T_{CELL} is the actual operating cell temperature calculated according to [39] as:

$$T_{CELL} = max\left(T_{AMB}; \frac{T_{AMB} + (NOCT - T_{AMB,NOCT}) \bullet \frac{GI}{GI_{NOCT}} \bullet \frac{\left(1-\eta_{PV,STC} \bullet \left(1-\gamma \bullet T_{CELL,STC}\right)\right)}{\tau_\alpha}}{1 + (NOCT - T_{AMB,NOCT}) \bullet \frac{GI}{GI_{NOCT}} \bullet \frac{\gamma \bullet \eta_{PV,STC}}{\tau_\alpha}}\right) \quad (3)$$

The main data and assumptions of the PV power plant are reported in Table 2.

3.2. Organic Rankine Cycle unit

The ORC unit herein considered is a 10 kWe hot-water-fed commercial unit operating with trans-1-Chloro-3,3,3-trifluoropropene (R1233zd) as working fluid. The ORC unit size was chosen considering the products available on the market, the amount of recoverable

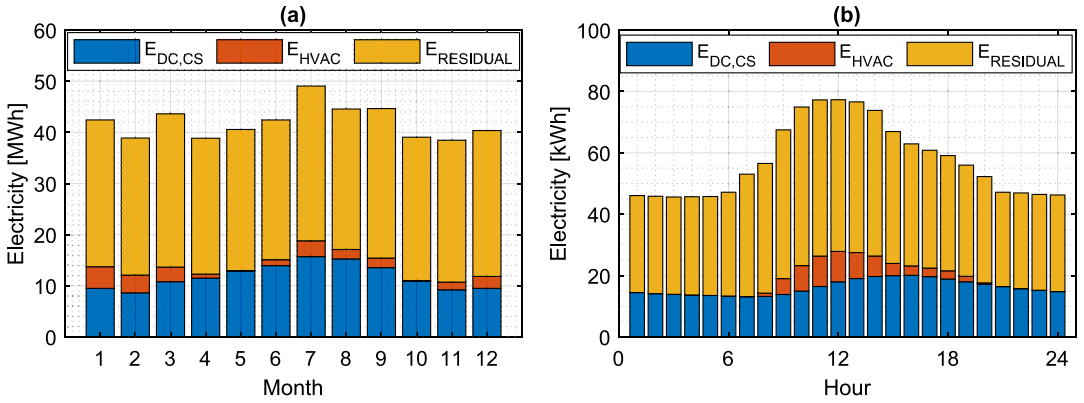

Fig. 1. Monthly (a) and average daily (b) electricity consumptions of the case study.

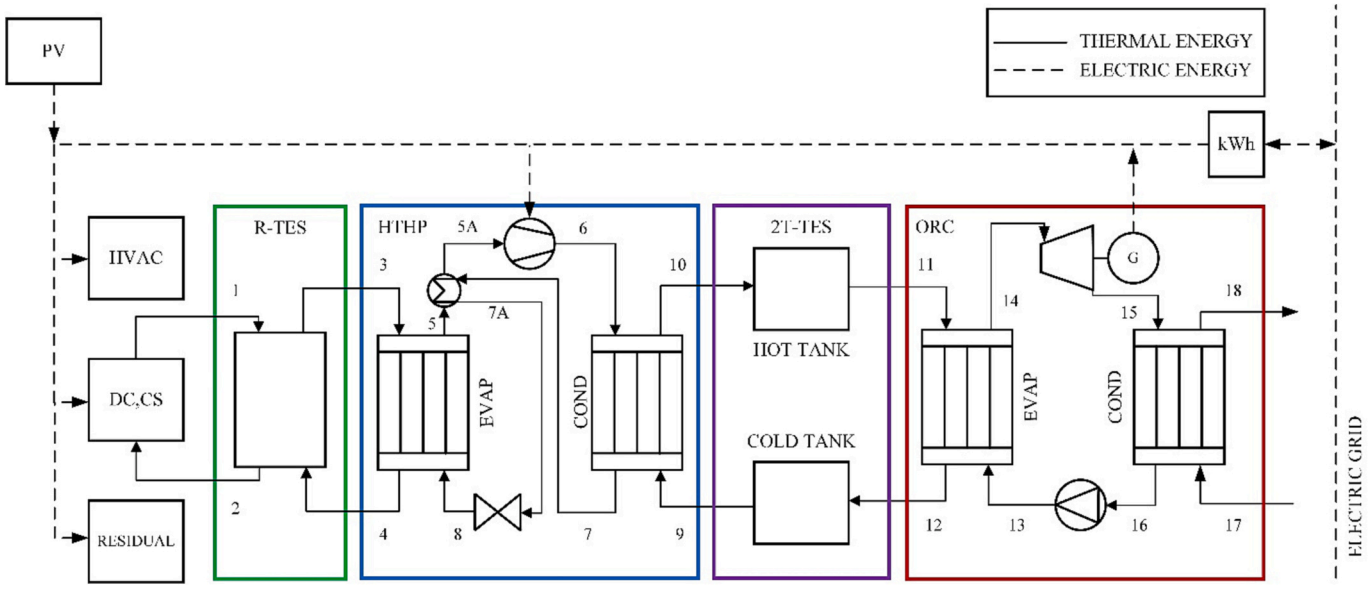

Fig. 2. Simplified diagram of the PV-PTES system.

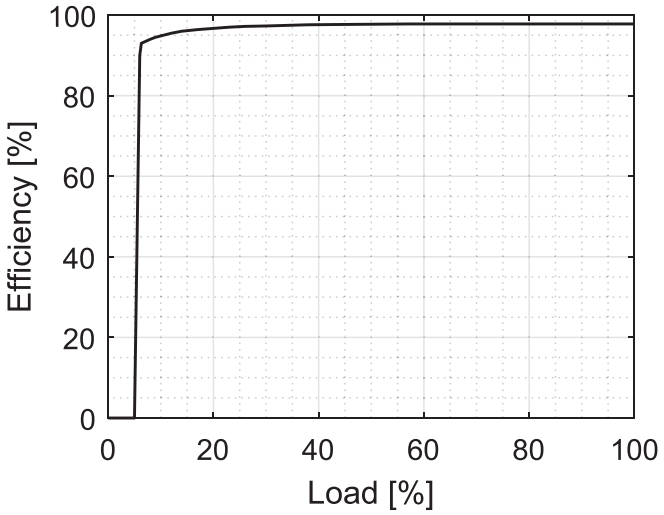

Fig. 3. Inverter efficiency as a function of the load.

Table 2
Photovoltaic power plant main data and assumptions.

Nominal power of a PV module [40]	360	Wp
Latitude	39.21	°
Tilt angle	0	°
Azimuth angle	15	°
Derating factor (f_{PV})	0.90	–
Nominal inverter efficiency (η_{INV})	0.978	–
STC conversion efficiency of a module ($\eta_{PV,STC}$)	0.221	–
STC cell temperature ($T_{CELL,STC}$)	25	°C
Net Operative Cell Temperature (*NOCT*)	41.5	°C
Ambient temperature at NOCT conditions ($T_{AMB,NOCT}$)	20	°C
Global Solar Irradiation at NOCT conditions (GI_{NOCT})	800	W/m^2
Solar transmittance and absorptance (τ_α)	0.9	–
Temperature correction factor (γ)	$-0.29{\cdot}10^{-2}$	1/K

Table 3
ORC unit main data.

Nominal power	10	kW
Heat source in-out temperatures (2T-TES)	98–68	°C
Thermal power input	150	kW
Cold source in-out temperature (air cooled condenser)	25–30	°C
Turbine isentropic efficiency [43]	0.80	–
Pump efficiency [43]	0.70	–

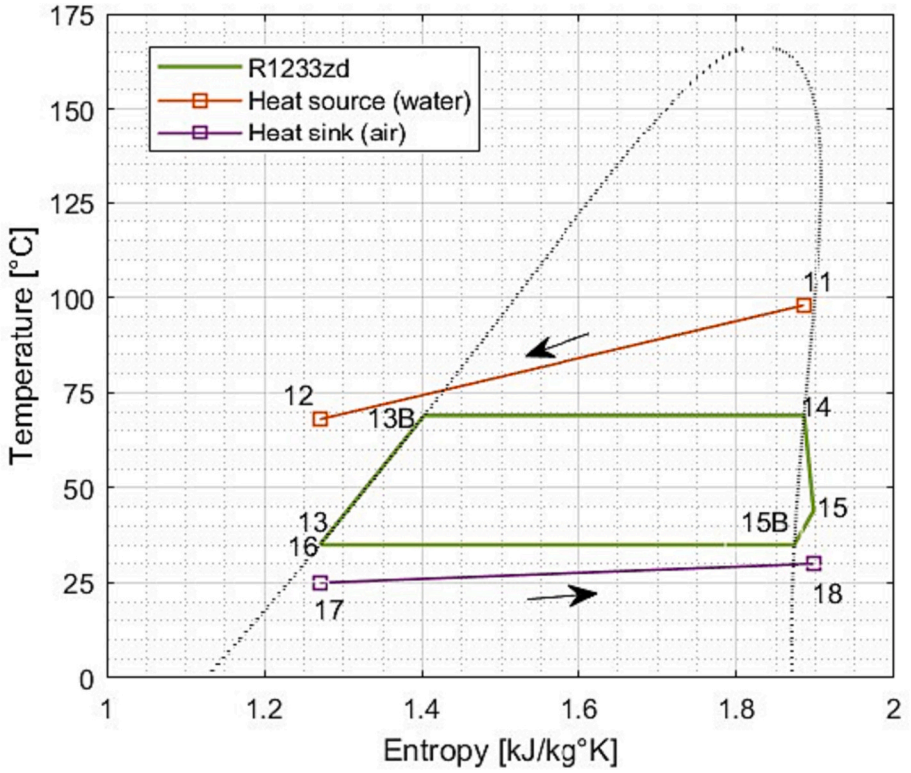

Fig. 4. ORC cycle in the temperature-entropy (T-s) diagram.

Table 4
ORC cycle thermodynamic values (R1233zd).

Point	Temperature [°C]	Pressure [bar]	Specific enthalpy [kJ/kg]	Specific entropy [kJ/kgK]
16	35	1.8	273.7	1.27
13	35	5.0	274.1	1.27
13B	69	5.0	316.9	1.40
14	69	5.0	482.3	1.88
15	44	1.8	467.2	1.89
15B	35	1.8	459.6	1.87

heat energy, the surplus PV production, as well as the size of the R-TES and 2T-TES. According to the manufacturer's technical data sheet [41], the considered ORC unit ensures the nominal power output of 10 kWe for heat source temperatures within the range 70–120 °C. Accordingly, the temperature of the Hot Tank of the 2T-TES system (later described in Section 3.3) was set to 100 °C. Based on the thermodynamic properties of the fluid [42] and some additional assumptions reported in Table 3, the operating cycle of the ORC unit was simulated, with no regeneration nor superheating, obtaining a nominal conversion efficiency η_{ORC} = 0.07. A turbine isentropic efficiency of 0.80 and a pump efficiency of 0.70 were considered, according to Chen et al. [43]. These values are also centred within the range of the parametric analysis carried out by Hu et al. [31]. In accordance with the results obtained by Dong et al., Weitzer et al. and Fatigati et al. [44–46], the nominal ORC efficiency varies within a range between 0.03 and 0.09 with changing in the input temperature of the heat source from the lowest to the highest limits of acceptability. The main thermodynamic points of the cycle are shown in Fig. 4 and reported in Table 4.

3.3. Thermal Energy Storage system

Thermal Energy Storage systems were modelled with a zero-dimensional approach, under the hypothesis of a perfect mixing. The R-TES is a single tank open-system with dual mass flow loops, while the 2T-TES is a two-tank open system. Unlike the 2T-TES, the mass level within the control volume of the R-TES is constant. For this reason, according to Raccanello et al. [47], the R-TES dynamic behaviour was described by the time evolution of the temperature inside the tank (T_{R-TES}) calculated by solving Eq. (4):

$$M_{R-TES} \bullet c \bullet \frac{dT_{R-TES}}{dt} = \dot{m}_{H,in} c_p \left(T_{H,in} - T_{R-TES}\right) + \dot{m}_{C,in} c_p \left(T_{C,in} - T_{R-TES}\right) - \dot{Q}_L \quad (4)$$

The time variation of the energy stored in the tank is determined by the enthalpy difference of the hot and cold mass flows ($\dot{m}_{H,in}$, $\dot{m}_{C,in}$) passing through the tank and by its thermal losses ($\dot{Q}_L$). The 2T-TES dynamic was modelled by solving the mass (5) and energy (6) balances:

$$\frac{dM_{2T-TES}}{dt} = \dot{m}_{TANK,in} - \dot{m}_{TANK,out} \quad (5)$$

$$M_{2T-TES} \bullet c_p \bullet \frac{dT_{2T-TES}}{dt} = \dot{m}_{,in} c_p \left(T_{,in} - T_{2T-TES}\right) - \dot{Q}_L \quad (6)$$

As suggested by Smallbone et at. [51], the thermal losses ($\dot{Q}_L$) for the two storage systems (2T-TES and R-TES) were calculated through a daily self-discharge rate of 1 % with respect to the stored energy.

3.4. High Temperature Heat Pump

The HTHP was modelled by increasing the size and reducing the temperature lift with respect to the one designed by CHESTER [33]. Based on the thermodynamic properties of the considered R-1233zd(E) fluid [42] and assuming a compressor isentropic efficiency of 0.80 [31] and an overall electromechanical efficiency of 0.95, the operating cycle of the HTHP unit was simulated obtaining a design Coefficient of Performance (COP) of 4.27 for a temperature lift of 65 °C. Although high evaporation temperatures allow to achieve high η_{RT}, as reported by Hu et al. [31], in the present case the evaporation temperature was

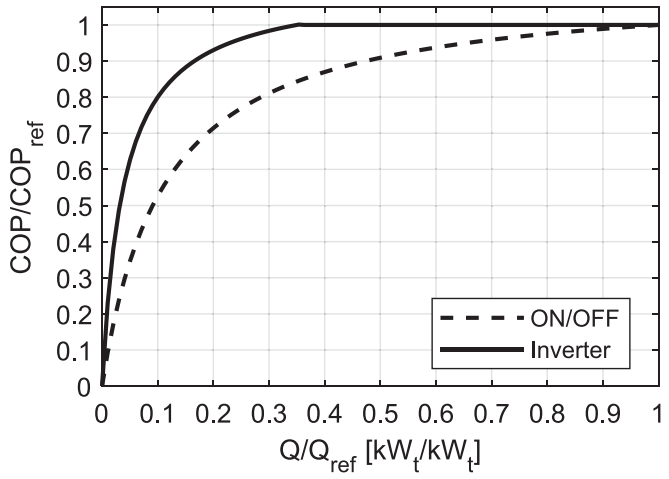

Fig. 5. Generalized COP profile (variation as a function of the load).

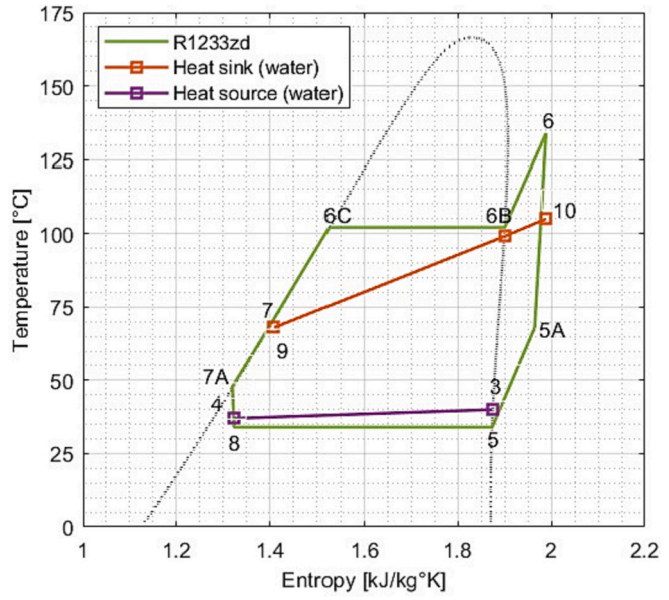

Fig. 6. HTHP cycle in the temperature-entropy (T-s) diagram.

Table 5
HTHP cycle thermodynamic values (R1233zd).

Point	Temperature [°C]	Pressure [bar]	Specific enthalpy [kJ/kg]	Specific entropy [kJ/kgK]
5A	68	1.8	488.4	1.96
6	134	10.9	536.6	1.99
6B	102	10.9	502.2	1.90
6C	102	10.9	361.8	1.53
7	71	10.9	319.6	1.41
7A	48	10.9	290.0	1.32
8	34	1.8	290.0	1.32
5	34	1.8	458.9	1.87

constrained by the temperature of the low-enthalpy waste thermal energy. When operating under partial load, the COP was assumed to vary according to the generalized COP profile reported in Fig. 5 (inverter operated HP compressor), calculated as described by UNI EN 14825:2022 [48]. Values of the thermodynamic properties of the characteristic points of the HTHP cycle are graphed in Fig. 6 and reported in Table 5.

Table 6
Heat exchangers main data.

HE	T in-out (hot side) [°C]	T in-out (cold side) [°C]	ΔT_{pp} [°C]	Overall heat transfer coefficient [kW/m^{2}K]
R-TES | HTHP	40–37	34–34	3	3.5
HTHP | 2T-TES	134–71	68–105	3	3.5
2T-TES | ORC	98–68	35.2–69	5	3.5

3.5. Heat Exchangers

Every heat exchanger herein considered was sized as a counterflow brazed plate unit, considering a steady-state energy balance, and neglecting thermal losses. Main HEs data are reported in the following Table 6.

As known, the assumed pinch-point temperature differences (ΔT_{pp}) influence the η_{RT} and consequently, the overall system performance. Reducing ΔT_{pp} values also entails cost increments associated with the increase of heat exchange surfaces. The influence of the ΔT_{pp} for the HE ORC-side and the HE HTHP-side on the system performance and on the LCOS was studied by Hu et al. [31] as well as by Iqbal et al. [49]. Both studies conclude that, for a Carnot battery similar to the one under consideration, the benefits on η_{RT} of reducing the ΔT_{pp} below the conventional 5 °C are reasonable in terms of Levelized Cost of Storage (LCOS) only for the HTHP-side HEs. For this reason, in the present study a $\Delta T_{pp} = 3$ °C was assumed for the HTHP-side HEs, while a slightly higher value of $\Delta T_{pp} = 5$ °C was assumed for the ORC-side HE.

4. Performance indicators

The overall performance of the PV-PTES system was evaluated using conventional energy and economic performance indicators, such as the energy self-sufficiency (SS), the energy self-consumption (SC), the round-trip efficiency (η_{RT}), the Levelized Cost of Storage (LCOS) as well as the Grid Impact (GI) index [54], an energy indicator herein reformulated. The performance indicators are defined with reference to the energy flows shown in Fig. 7. The energy produced by the PV system E_{PV} is split into $E_{PV,SC}$ (Self Consumed) and $E_{PV,G}$ (fed into the grid), while $E_{PV,SC}$ is further split into $E_{PV,SC,PTES}$ (the share of $E_{PV,SC}$ which is consumed by the heat pump) and $E_{PV,SC,U}$ (the share of the $E_{PV,SC}$ which is directly consumed by the user). The sum of the energy produced by the ORC unit ($E_{ORC,U}$) and $E_{PV,SC,U}$ gives $E_{SS,U}$, which is the energy self-supplied to the user. The total user demand E_U is given by the sum of the energy from the grid $E_{G,U}$ and $E_{SS,U}$.

The self-sufficiency index, defined by Eq. (7), quantifies the extent to which the system is capable to meet its own energy demand without relying on external sources. It is calculated by the ratio of the energy self-supplied to the user and the overall energy demand of the user:

$$SS = \frac{E_{SS,U}}{E_U} = \frac{E_U - E_{G,U}}{E_U} \tag{7}$$

The self-consumption index, as reported in Eq. (8), is obtained by dividing the amount of energy produced and self-consumed by the total energy generated by the PV system:

$$SC = \frac{E_{PV,SC}}{E_{PV}} = \frac{E_{PV} - E_{PV,G}}{E_{PV}} \tag{8}$$

The system round-trip efficiency, is the ratio of the energy output and the energy input in a closed-loop cycle:

$$\eta_{RT} = \frac{E_{ORC,U}}{E_{PV,SC,PTES}} = \frac{E_{ORC,U}}{E_{HTHP}} \tag{9}$$

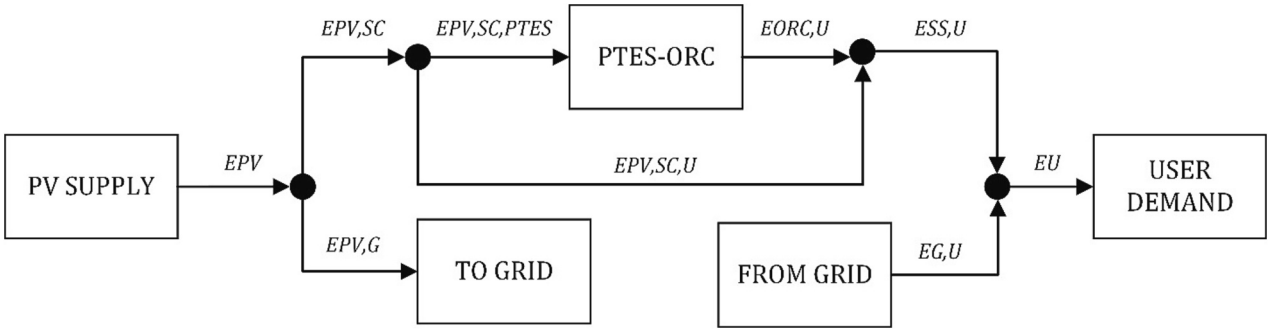

Fig. 7. Diagram of energy flows.

where $E_{ORC,U}$ is the ORC energy production and E_{HTHP} is the energy consumed by the HTHP unit (that equals $E_{PV,SC,PTES}$).

When comparing alternative solutions, systems that enable achieving the highest levels of SS and SC usually represent the best solution. This is true not only from the perspective of plant owners, but also from that of the grid operator, which take advantages of reduced impact on the grid. In fact, greater SC shares correspond to reduced energy feed-ins, whereas increased SS levels result in diminished grid energy withdrawals. Apart from the systems specifically conceived to provide flexibility services, both feed-ins and withdrawals are usually exchanges of energy with the grid, and therefore cause of increased grid impact. As stated by I.E.A. [1], in a global scenario of increasing RES penetration and energy demand, systems that generate the lowest grid impact are going to be preferred. Even if SS and SC give someway a measure of the grid impact of the system, a more specific index can be very useful for the comparison of different options. For this reason, the Grid Impact (*GI*) index [54] is herein reformulated and defined as:

$$GI = \frac{|E_{PV,G}| + |E_{G,U}|}{E_U} = \frac{|E_{PV}(1-SC)| + |E_U(1-SS)|}{E_U} \tag{10}$$

GI relates the absolute values of energy exchanges with the grid (feed-ins and withdrawals) to the overall user demand. The minimum impact on the grid corresponds to systems with the lowest values of GI, which is always greater than or equal to zero. The latter case (GI = 0) is represented by systems where all the energy required by the user is self-produced with no feed-ins. On the contrary, in a scenario without self-production systems, all the required energy is exchanged with the grid and therefore GI = 1. GI values greater than 1 represents those situations where energy exchanges exceed the energy demand.

Table 7
LCOS assessment assumptions[a].

Parameter	Value	Ref.
Pumps CAPEX ($)	$1,120 \bullet \dot{E}_{el,pump}^{0.8}$	[52]
Heat exchangers CAPEX ($)	$2,143 \bullet A_{HX}^{0.514}$	[52]
Turbine and generator CAPEX ($)	$4,405 \bullet \dot{E}_{el,turb}^{0.8} + 10^7 \left(\frac{\dot{E}_{el,gen}}{1.6 \bullet 10^5}\right)^{0.7}$	[52]
Compressor CAPEX ($)	$98,400 \left(\frac{\dot{E}_{el,comp}}{250}\right)^{0.46}$	[31]
2T-TES and R-TES tanks CAPEX ($)	$1,200 \bullet V$	[51,53]
All components' OPEX ($)	$0.015 \bullet CAPEX$	[31]
Lifetime (years)	30	[16]
Discount factor *r* (%)	5	[31]
Unitary cost for electricity c_{el} ($/kWh)	0	

[a] Power in kW, area in m^2 and volume in m^3.

The system Levelized Cost of Storage (LCOS) [50,51] is calculated as:

$$LCOS = \frac{CAPEX + \sum_{i=1}^{L} \frac{A_i}{(1+r)^i}}{\sum_{i=1}^{L} \frac{E_{ORC,U}}{(1+r)^i}} \tag{11}$$

where *CAPEX* are the capital expenditures and A_i and $E_{ORC,U}$ are, respectively, the annual cost and the amount of electricity discharged by the storage system for each year *i* of the lifetime *L*, both discounted using the discount factor *r*. A_i is given by:

$$A_i = OPEX + c_{el} \bullet E_{PV,SC,PTES} \tag{12}$$

where *OPEX* is the yearly operation cost and c_{el} is the unitary cost for buying the electricity $E_{PV,SC,PTES}$ used for charging. Table 7 reports the assumptions made for the LCOS assessment. Since the considered PTES system is charged with surplus energy coming from the PV, c_{el} was assumed null.

5. Results

The results reported in this section were obtained based on the actual annual consumption data of the case study with hourly resolution.

The performance of the PV-PTES energy system applied to the case study was assessed by varying three design parameters, specifically the size of the HTHP (expressed as its nominal electric power) and the storage volume of the two TES systems (2T-TES and R-TES). The sensitivity analysis was conducted by varying the electrical power of the HTHP from 10 to 60 kW and the capacity of both the 2T-TES and R-TES from 12 to 48 m^3. Larger storage volumes were not considered to avoid unrealistic space occupation. The PV-PTES system performance was also compared with a reference scenario (named "PV-only") where only the PV plant is implemented. Results are initially presented considering a PV system with a nominal size of 350 kWp. This size was selected to achieve an annual PV energy production (504 MWh) equal to the annual user energy demand (502 MWh). Successively, results are shown for a wider PV power range, from 100 kWp to 500 kWp. The generalized PV production profile is reported in Fig. 8(a) on a monthly basis and in Fig. 8(b) on a daily basis for three typical seasonal days.

5.1. Influence of HTHP, 2T-TES and R-TES size

The following figures show the trend of the five performance indicators SS, SC, η_{RT}, GI, and LCOS, as a function of the HTHP size, for different TES capacities and a PV size of 350 kWp.

The SS ratio is displayed in Fig. 9 for the different PV-PTES cases, as well as for the PV-only scenario. It can be immediately noticed that in comparison to the PV-only scenario, the PV-PTES system is able to increase the SS level up to a maximum of 6 percentage points (55.0 % vs 49.0 %). In fact, the PV-PTES is basically an addition of a storage system to the PV-only scenario, which allows for more solar energy to be self-consumed, stored, and later consumed. For a given PV yearly

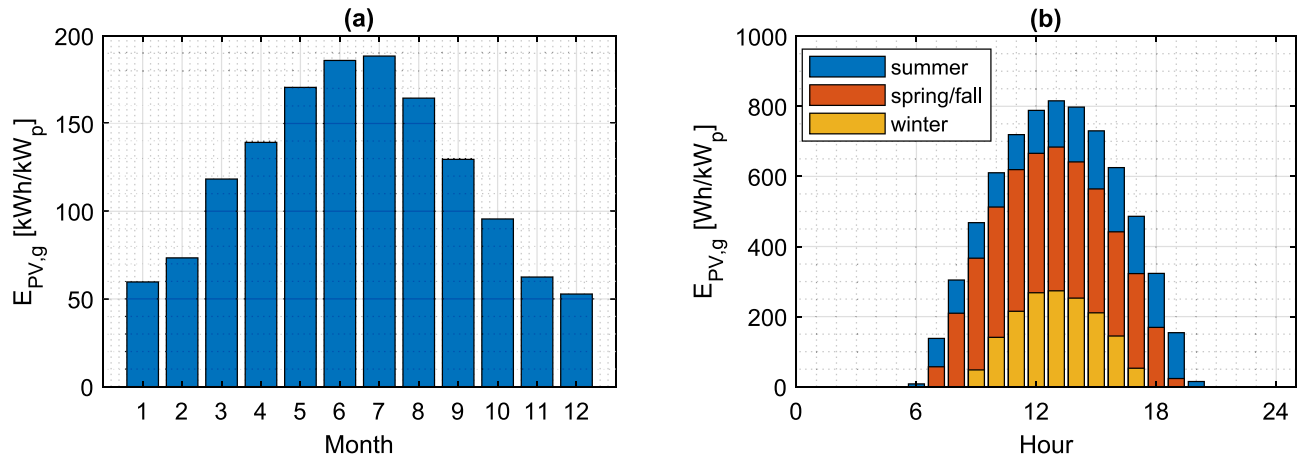

Fig. 8. Monthly (a) and daily (b) generalized PV production.

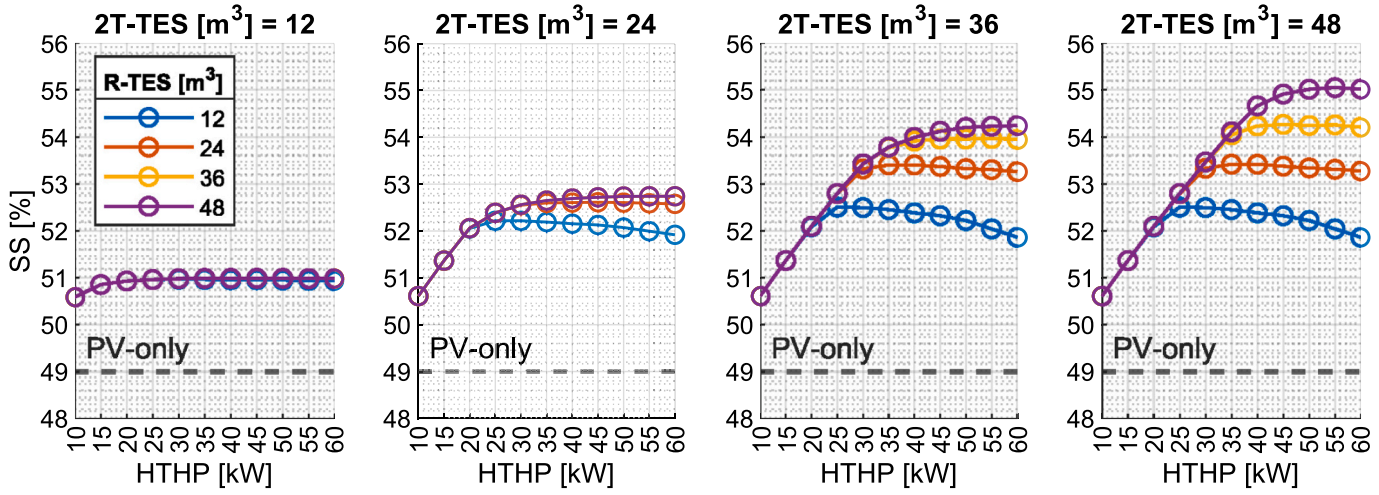

Fig. 9. Self-Sufficiency (SS) rate varying the size of the HTHP and the capacity of the two TESs (PV = 350 kWp).

production, a simultaneous rise in R-TES and 2T-TES sizes results in an increase of SS. A larger R-TES means that more energy is available at the heat sink of the HTHP, just as a larger 2T-TES means that more energy is deliverable at the heat source of the HTHP. If more energy is stored for a future ORC production, SS shares are consequently higher. Obviously, the amount of energy that can be stored in the R-TES is constrained by the maximum energy recovery achievable from the data center cooling system. Similarly, the maximum energy that can be stored in the 2T-TES depends (apart from the energy available at the heat sink) on the available surplus energy from PV, which powers the HTHP. With

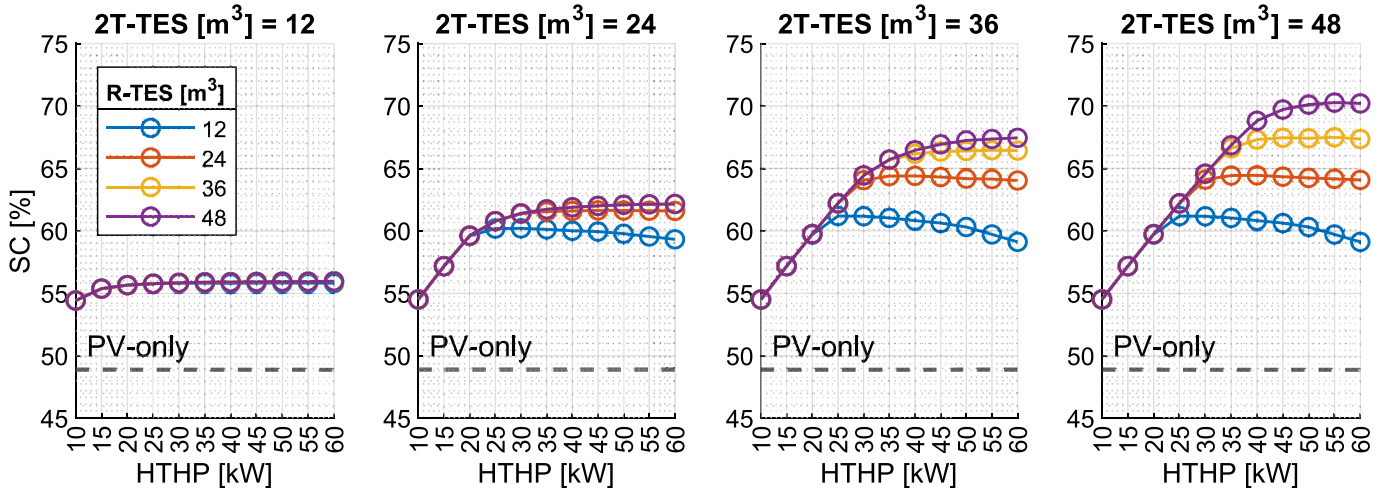

Fig. 10. Self-Consumption (SC) rate varying the size of the HTHP and the capacity of the two TESs (PV = 350 kWp).

reference to the influence of 2T-TES and R-TES capacities on SS, it's also interesting to note the curve distancing as the 2T-TES capacity increases. In fact, for the lowest considered 2T-TES capacity, all SS curves overlap due to the insufficient capacity of the 2T-TES to allow the increase of the ORC production alongside other parameters growth. As 2T-TES capacity increases, the SS curves spread apart because it becomes possible to utilize larger amounts of both the waste heat from the data center (with a larger R-TES) and the power from the PV system (with HTHPs operating closer to their design power and at a lower degree of modulation).

With reference to the influence of the HTHP size on SS, it can be noted that an increase in this size does not always lead to an increase in SS. This is particularly evident for 2T-TES capacities of 36 m^3 and 48 m^3, where three regions can be clearly observed: a first region where the influence of HTHP size on SS is strong (steep positive slope), a second region with no influence (horizontal slope) and a third region with a gentle negative slope. Within the first region, the influence of HTHP size on SS is strong because in this region the size of the HTHP is considerably smaller compared to the average power overproduction of the considered PV system. Therefore, even a slight increase in the HTHP size yields substantial benefits in terms of energy stored in the 2T-TES, and therefore produced by the PTES section. The absence of influence of HTHP size on SS of the second region is due to the fact that the HTHP is equipped with an inverter, allowing modulation down to a partial load of 35 % without compromising the COP. Therefore, larger HTHPs operate with significant modulation but comparable COP values to the smaller ones, resulting in the same SS rate. In the third region, SS slightly decreases by increasing the size of the HTHP (this is very clear for R-TES = 12 m^3) because the average partial load of the HTHP is under the abovementioned 35 % and therefore the lower COP negatively affects the energy output.

A final interesting outcome of the analysis of the SS trend is that, for every combination of 2T-TES and R-TES, there is an HTHP size that maximizes self-sufficiency. This HTHP size represents the minimum capacity needed to fully utilize the considered storage volumes and the available PV energy.

Fig. 10 displays the trend of self-consumption varying the size of the HTHP and the capacity of the two TESs (PV = 350 kWp). As it can be seen, the SC trend is very similar to that of SS. In fact, the self-supplied energy directly depends on the self-consumed energy, being the former an energy transformation of the latter characterized by the round-trip efficiency shown in Fig. 11. As it can be observed, the SC of the PV-PTES increases with the three design parameters from a minimum of 55 % up to a maximum of 70 %. In the PV-only scenario, the SC is 49 %. The maximum of *SC* is obtained for 2T-TES = 48 m^3, HTHP = 55 kWe and R-TES = 48 m^3, with 21 percentage points increase with respect to the PV-only scenario. Fig. 11 demonstrates that, except for minor differences, the only parameter that influences η_{RT} is the size of HTHP. In fact, for larger HTHP sizes, partial load operating conditions are more frequent, leading to lower COP values.

Fig. 12 shows the behaviour of the GI index while varying the size of the HTHP and the capacity of the two TES systems. The GI index of the PV-PTES is within the range 0.75–0.95, meaning that for every kWh of user demand, the energy exchanged with the grid is within the range 0.75–0.95 kWh. The lowest GI value is obtained for the combination of the design parameters that ensures highest values of SC and SS: this happens because a high SC means low grid feed-ins as well as a high SS means low withdrawals. Compared to a scenario without any internal energy production system, in which GI would be unitary, the PV-PTES solution allows to a beneficial reduction of grid impact. The GI reduction achievable with the PV-PTES solution is even more favourable if compared to the PV-only scenario, whose GI = 1.02. In fact, the PV-only scenario increases the grid impact due to energy feed-ins.

Finally, Fig. 13 shows the LCOS behaviour with the variation of the size of the HTHP and the capacity of the two TES systems. The LCOS initially decreases by increasing the HTHP power because the energy production of the ORC increases more than the HTHP relative costs. The LCOS reaches a minimum (particularly evident for each curve of 2T-TES = 12 m^3). After that minimum, the LCOS values increase because the growth in HTHP cost is not compensated by a similar increase in ORC production.

Yearly overall results for both the PV-only scenario and the lowest (Case 1), intermediate (Case 2), and the highest (Case 3) combinations of the considered PV-PTES design parameters are reported in Table 8. For the considered range of design parameters, E_{ORC} is included in the range 8 MWh–30 MWh, SS shares are comprised between 49.0 % (PV-only) and 55.1 % (PV-PTES), SC shares are in the range 48.9 % (PV-only) and 70.3 % (PV-PTES) and GI between 0.75 (PV-PTES) and 1.02 (PV-only).

To evaluate the influence of a different demand profile on the system's performance, the existing demand profile was modified through hourly randomization within the range of 50–150 % and simulation was carried out for the highest combinations of the considered PV-PTES design parameters. The results, which are reported in the last column (Case 3*) of Table 8, show maximum differences of 1.5 %, compared to Case 3, for each considered parameter.

5.2. Seasonal influence

Fig. 14 shows the influence of the seasonality on the energy performance of the PV-PTES system (SS, SC and GI) for the combination of values of HTHP size and TES capacities that maximizes the performance indicators (HTHP = 55 kWe, 2T-TES = 48 m^3, R-TES = 48 m^3) for the considered PV size of 350 kWp.

Fig. 14(a) reveals that the SS rate varies from a minimum of approximately 45 % (winter and autumn) to a maximum of around 65 % (spring and summer). This seasonal fluctuation is explained by examining the seasonal PV production (E_{PV}) reported in Fig. 14(b). The higher PV production during spring and summer leads to an increase of the self-consumed energy ($E_{PV,SC}$), resulting in higher energy self-supplied to the user ($E_{SS,U}$). The seasonal SC trend in Fig. 14(b) also indicates that during winter and autumn, the PV-PTES system can self-consume (and store) up to the 86 % of the PV energy. In contrast, during spring and summer, the system reaches an SC value around 60 %. The impact on the

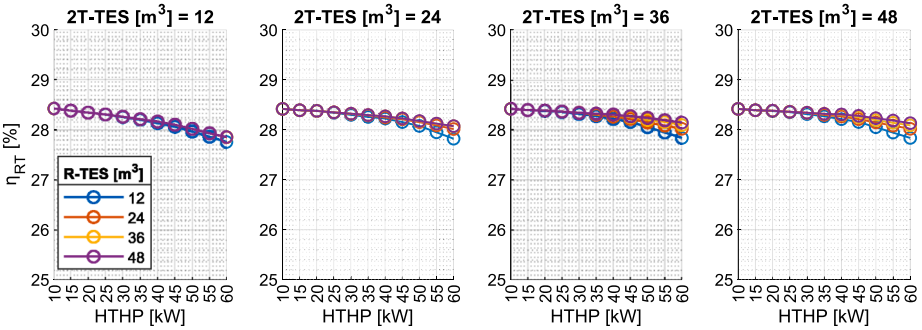

Fig. 11. Round-trip efficiency (η_{RT}) varying the size of the HTHP and the capacity of the two TESs (PV = 350 kWp).

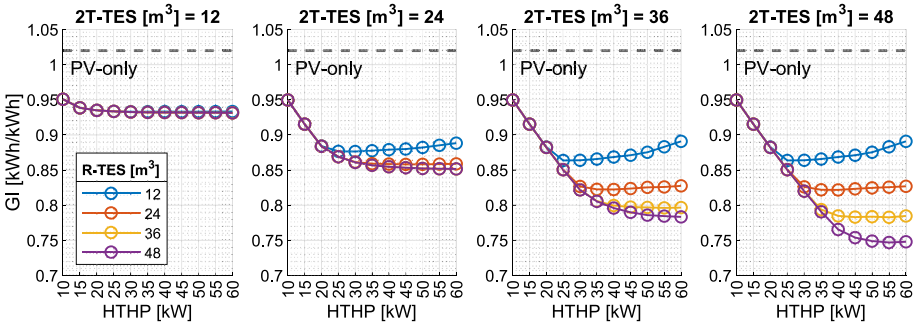

Fig. 12. Grid Impact (GI) varying the size of the HTHP and the capacity of the two TESs (PV = 350 kWp).

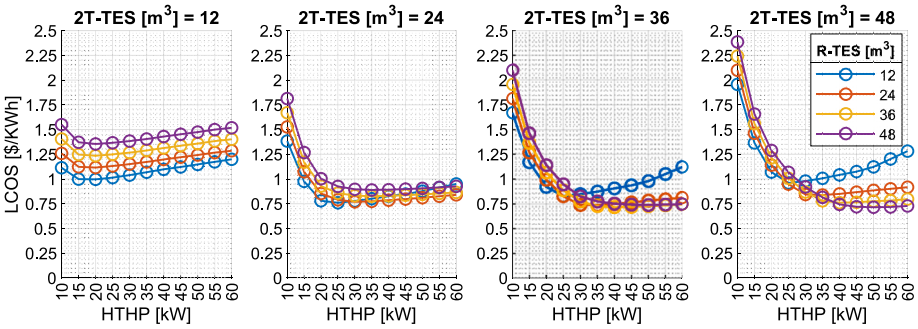

Fig. 13. Levelized Cost of Storage (LCOS) varying the size of the HTHP and the capacity of the two TESs (PV = 350 kWp).

Table 8
Yearly overall performance (PV = 350 kWp).

Scenario		PV-only	PV-PTES			
			Case 1	Case 2	Case 3	Case 3*
HTHP	kWe	0	10	35	55	55
2T-TES	m^3	0	12	36	48	48
R-TES	m^3	0	12	24	48	48
Photovoltaic production (E_{PV})	MWh	504.1	504.1	504.1	504.1	504.1
PV energy directly consumed ($E_{PV,SC,U}$)	MWh	246.5	246.5	246.5	246.5	243.8
PV energy consumed by HTHP ($E_{PV,SC,PTES}$)	MWh	0	27.9	78.1	107.7	108.2
PV energy fed into the grid ($E_{PV,G}$)	MWh	257.6	229.7	179.5	149.9	152.1
ORC unit production ($E_{ORC,U}$)	MWh	0	7.9	22.1	30.4	30.5
Electricity purchased from the grid ($E_{G,U}$)	MWh	256.5	248.5	234.4	226.1	228.6
Self-Sufficiency (SS)	%	49.0	50.6	53.4	55.1	54.5
Self-consumption (SC)	%	48.9	54.4	64.4	70.3	69.8
Round Trip efficiency (η_{RT})	%	–	28.4	28.3	28.2	28.2
Grid Impact (GI)	–	1.02	0.95	0.82	0.75	0.76
Levelized Cost of Storage (LCOS)	$/kWh	–	1.10	0.81	0.72	0.72

* Randomized demand profile.

grid of these SS and SC fluctuations is shown in Fig. 14(c): the GI values are higher during spring and summer, because the ratios of $E_{PV,G} + E_{G,U}$ to E_U are higher compared to winter and autumn, mainly due to the contribution of $E_{PV,G}$.

5.3. Influence of PV system size

The following figures show the influence of the PV size on the energy performance of the PV-PTES system (SS, SC and GI) in comparison with the corresponding PV-only scenario. Results are shown for the combination of values of HTHP size and TES capacities that maximizes the performance indicators herein considered (HTHP = 55 kWe, 2T-TES = 48 m^3, R-TES = 48 m^3).

Fig. 15(a) displays the SS values of both the PV-PTES system and the PV-only scenario, while Fig. 15(b) displays the percentage increase of SS achievable with the PV-PTES system compared to the SS of the PV-only scenario. As expected, SS values increase along with the PV system size for both PV-PTES and PV-only cases, passing from 27.5 % (PV-only, 100 kW) up to 58 % (PV-PTES, 500 kW). The influence of PV size on SC decreases as PV size increases for both cases, as shown by the SC trends, which tend to become horizontal for higher PV values. For the PV-only scenario, this occurs because the system reaches its maximum level of SS, that is the covering of the entire light-hours energy demand. For the PV-PTES scenario, the maximum level of SS of the PV-only case is increased by the energy production during the night hours, up to the maximum represented by the storage capacity. The percentage increase in SS of the PV-PTES shown in Fig. 15(b) reaches its maximum for the highest PV size, because the more the PV size, the more the excess energy that is stored (and consequently produced) rather than being fed into the grid.

On the contrary to SS trend, SC values (Fig. 16) obviously decrease as the PV size grows, and PV production exceeds the demand. The maximum SC values (close to 100 %) are obtained for the PV-PTES solution and a size of PV of both 100 and 150 kW, while the minimum SC

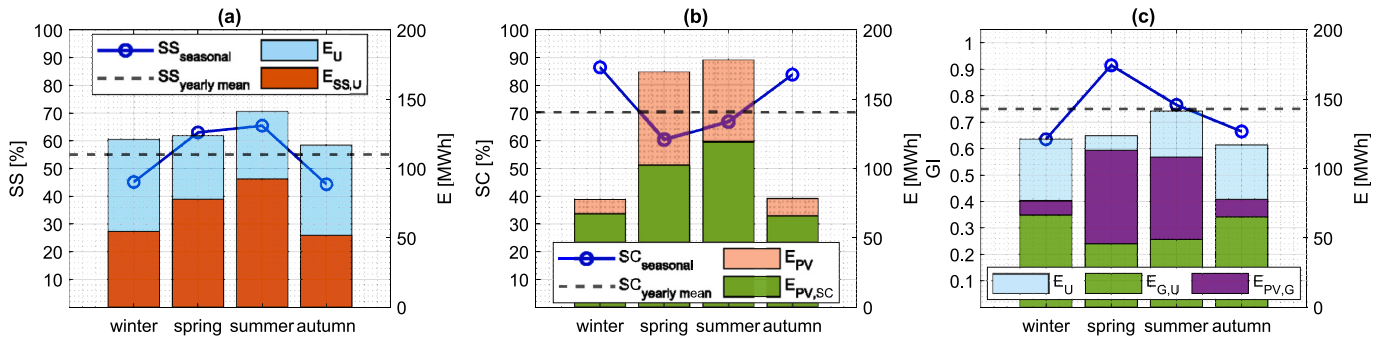

Fig. 14. Seasonal trend of Self-Sufficiency (SS) (a), Self-Consumption (SC) (b) and Grid Impact (GI) (c) rate (PV = 350 kWp, HTHP = 55 kWe, 2T-TES = 48 m^3, R-TES = 48 m^3).

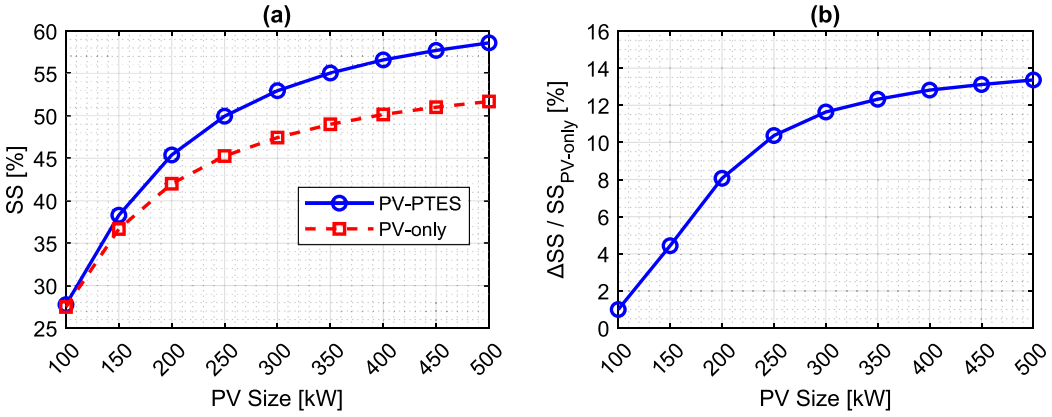

Fig. 15. Self-Sufficiency (SS) rate varying the size of the PV system (HTHP = 55 kWe, 2T-TES = 48 m^3, R-TES = 48 m^3).

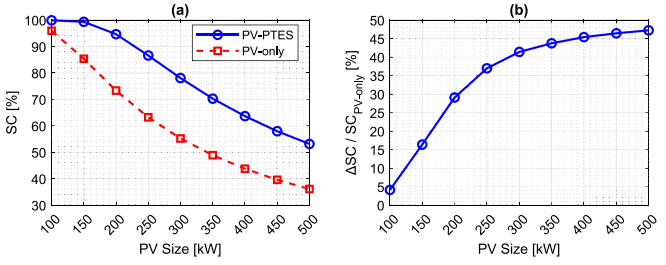

Fig. 16. Self-Consumption (SC) rate varying the size of the PV system (HTHP = 55 kWe, 2T-TES = 48 m^3, R-TES = 48 m^3).

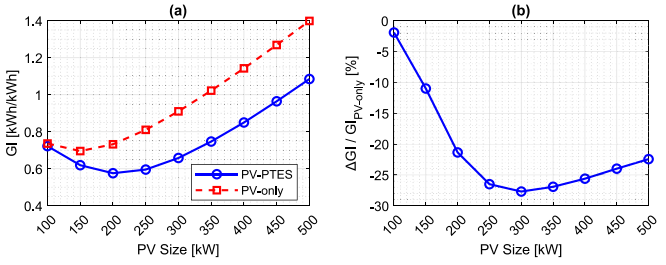

Fig. 17. Grid Impact (GI) varying the size of the PV system (HTHP = 55 kWe, 2T-TES = 48 m^3, R-TES = 48 m^3).

(36 %) is obtained for the PV-only case (PV size of 500 kW). It can be generally noted that SC shares of the PV-PTES system are always higher than those of the PV-only. When focusing on the percentage increase in SC of the PV-PTES system with respect to the PV-only (Fig. 16(b)), it is evident that the highest increases are obtained for powerful PV systems, because of the same reasons discussed for SS.

Finally, the GI index is shown for both the PV-PTES system and the PV-only scenario in Fig. 17(a), and as the percentage decrease achievable with the PV-PTES solution compared to the PV-only scenario in Fig. 17(b). It is firstly notable that exists a PV size which minimizes GI, represented by 150 kW for PV-only and 200 kW for PV-PTES solutions. However, the minimum GI of the PV-only solution (around 0.7) is considerably higher than that of the PV-PTES one (0.6). In absolute terms, to the minimum GI of the PV-only scenario (PV = 150 kW) corresponds around 50 MWh of more energy exchanges with the grid with respect to the minimum GI of the PV-PTES solution (PV = 200 kW). The initial decrease in GI as the PV size increases is due to the fact that the self-sufficiency levels increase considerably (mainly due to strongly reduced withdrawals), while the self-consumption levels remain very high (almost zero feed-ins for the PV-PTES system and very low for the PV-only). Beyond the minimum, the GI values rise because the self-consumption levels decrease (the feed-ins increase) while the self-sufficiency growth is slower (due to slightly reduced withdrawals).

In conclusion, in a future scenario, the analysis of the GI index can be very useful to compare alternative energy storage systems with the aim of favouring those that generate the lowest grid impacts. In fact, in the specific case of Fig. 17(a–b), the lowest absolute value of GI is given by Fig. 17(a), while the maximum reduction in GI can be easily identified in Fig. 17(b), and it is represented by the PV-PTES system with a PV size of 300 kW, in which the percentage decrease compared to a same size PV-only is around 28 %.

6. Conclusions

This paper investigated the performance of a PTES system coupled with a PV plant for small scale applications which represents a possible energy storage complement to electrochemical battery systems. The PV-PTES system was designed for enhancing the self-sufficiency of a real

energy context. The influence of the seasonality as well as of the main design parameters (PV size, heat pump size and capacities of the two thermal energy storage systems) on the system energy performance was assessed through the well-known indicators given by the energy self-sufficiency SS, the energy self-consumption SC, the system round-trip efficiency η_{RT} and the indicator GI, which quantifies the grid impact of the system. The influence of the main design parameters on the Levelized Cost of Storage was assessed as well.

The analysis highlighted several advantages of the proposed PV-PTES system with respect to a scenario only based on a PV system. In fact, for a given PV size, the PV-PTES solution allows to achieve an increase in SS within the range 1–14 % with respect to the PV-only option, as well as a SC increase within the range 5–47 % and a GI decrease within the range 2–28 %. The improvement introduced by the PTES section on energy self-sufficiency and energy self-consumption increases by increasing the PV size. The values of the grid impact index of the PV-PTES are always lower than those of the PV-only and for both solutions the GI trend presents a minimum representing the best trade-off between feed-ins and withdrawals. The improvement of the GI performance index is achieved despite the low PV-PTES round-trip efficiencies (around 28 %), mainly due to the low ORC unit efficiency, the high latent to sensible heat ratio of the ORC working fluid and the high temperature lift of the HTHP. The main energy performance indicators vary throughout the four seasons within a range of ±20 % with respect to their yearly mean values.

The study was also aimed to evaluate technological solutions complementary to batteries for small-scale energy storage solutions. The lowest LCOS for the case study is approximately 0.72 $/kWh, which today is considerably higher with respect to that of BESS [50]. However, in a future scenario, small-scale PV-PTES systems may potentially emerge as a viable solution, driven in part by the reduction in costs facilitated by the attainment of technological maturity as well as due to some favourable features such as low-capacity degradation over time, long operating life, reduced environmental impact and their suitability for multi-vector energy systems.

CRediT authorship contribution statement

Luca Migliari: Conceptualization, Data curation, Formal analysis, Methodology, Software, Writing – original draft, Writing – review & editing. **Mario Petrollese:** Conceptualization, Formal analysis, Methodology, Software, Writing – review & editing. **Giorgio Cau:** Formal analysis, Methodology, Supervision, Writing – review & editing. **Daniele Cocco:** Formal analysis, Methodology, Supervision, Writing – review & editing.

Declaration of competing interest

The authors declare that they have no known competing financial interests or personal relationships that could have appeared to influence the work reported in this paper.

Data availability

Data will be made available on request.

Acknowledgements

This paper forms part of a research project cofounded: under the National Recovery and Resilience Plan (NRRP), Mission 4 Component 2 Investment 1.3 - Call for tender No. 1561 of 11.10.2022 of Ministero dell'Università e della Ricerca (MUR); funded by the European Union – NextGenerationEU. Project code PE0000021, Concession Decree No. 1561 of 11.10.2022 adopted by Ministero dell'Università e della Ricerca (MUR), CUP F53C22000770007, according to attachment E of Decree No. 1561/2022, Project title "Network 4 Energy Sustainable Transition – NEST" and under the project entitled "e.INS, Ecosystem of Innovation for Next Generation Sardinia", Project funded under the NATIONAL RECOVERY AND RESILIENCE PLAN (PNRR) - MISSION 4 COMPONENT 2, "From research to business" INVESTMENT 1.5, "Creation and strengthening of Ecosystems of innovation" and construction of "Territorial R&D Leaders" (CUP F53C22000430001).

References

[1] Energy Transitions Require Innovation in Power System Planning – Analysis - IEA, n.d. https://www.iea.org/articles/energy-transitions-require-innovation-in-power-system-planning. (Accessed 4 October 2023).
[2] I. International Energy Agency, Renewable Energy Market Update - June 2023. www.iea.org/t&c/, 2023.
[3] Will More Wind and Solar PV Capacity Lead to More Generation Curtailment? – Renewable Energy Market Update - June 2023 – Analysis - IEA, n.d. https://www.iea.org/reports/renewable-energy-market-update-june-2023/will-more-wind-and-solar-pv-capacity-lead-to-more-generation-curtailment. (Accessed 19 September 2023).
[4] IRENA, Power system flexibility for the energy transition, in: Part 1: Overview for Policy Makers 2018, International Renewable Energy Agency, Abu Dhabi, 2018, pp. 1–48 (/-/media/Files/IRENA/Agency/Publication/2018/Nov/IRENA_Power_system_flexibility_1_2018.pdf?rev=472c42dcadb746a7b4f6132d5dbf470e (accessed October 4, 2023)).
[5] International Energy Agency, World Energy Outlook 2022. www.iea.org/t&c/, 2022.
[6] H. Nami, A. Arabkoohsar, Improving the power share of waste-driven CHP plants via parallelization with a small-scale Rankine cycle, a thermodynamic analysis, Energy 171 (2019) 27–36, https://doi.org/10.1016/J.ENERGY.2018.12.168.
[7] P. Neuman, M. Pokorny, W. Weiglhofer, Principles of smart grids on the generation electrical and thermal energy and control of heat consumption within the district heating networks, IFAC Proc. Volumes. 47 (2014) 1–6, https://doi.org/10.3182/20140824-6-ZA-1003.00553.
[8] L. Migliari, D. Micheletto, D. Cocco, Performance analysis of a diabatic compressed air energy storage system fueled with green hydrogen, Energies 16 (2023) 7023, 16 (2023) 7023, https://doi.org/10.3390/EN16207023.
[9] A. Benato, A. Stoppato, Pumped thermal electricity storage: a technology overview, Thermal Sci. Eng. Progr. 6 (2018) 301–315, https://doi.org/10.1016/j.tsep.2018.01.017.
[10] W.D. Steinmann, Thermo-mechanical concepts for bulk energy storage, Renew. Sustain. Energy Rev. 75 (2017) 205–219, https://doi.org/10.1016/j.rser.2016.10.065.
[11] World Energy Council, Energy Storage Monitor: Latest Trends in Energy Storage. www.worldenergy.org, 2019.
[12] World Energy Council, E-storage: shifting from cost to value—wind and solar applications. www.worldenergy.org, 2016.
[13] A. Zablocki, Energy Storage: Fact Sheet (Environmental and Energy Study Institute). https://www.eesi.org/papers/view/energy-storage-2019, 2019. (Accessed 17 March 2023).
[14] A.V. Olympios, J.D. McTigue, P. Farres-Antunez, A. Tafone, A. Romagnoli, Y. Li, Y. Ding, W.D. Steinmann, L. Wang, H. Chen, C.N. Markides, Progress and prospects of thermo-mechanical energy storage-a critical review, Progress Energy 3 (2020), https://doi.org/10.1088/2516-1083/abdbba.
[15] O. Dumont, V. Lemort, Mapping of performance of pumped thermal energy storage (Carnot battery) using waste heat recovery, Energy 211 (2020), 118963, https://doi.org/10.1016/J.ENERGY.2020.118963.
[16] G.F. Frate, L. Ferrari, P. Sdringola, U. Desideri, A. Sciacovelli, Thermally integrated pumped thermal energy storage for multi-energy districts: integrated modelling, assessment and comparison with batteries, J Energy Storage 61 (2023), 106734, https://doi.org/10.1016/J.EST.2023.106734.
[17] B. Kurşun, K. Ökten, Comprehensive energy, exergy, and economic analysis of the scenario of supplementing pumped thermal energy storage (PTES) with a concentrated photovoltaic thermal system, Energ. Conver. Manage. 260 (2022), 115592, https://doi.org/10.1016/J.ENCONMAN.2022.115592.
[18] I. Vorushylo, P. Keatley, N. Shah, R. Green, N. Hewitt, How heat pumps and thermal energy storage can be used to manage wind power: a study of Ireland, Energy 157 (2018) 539–549, https://doi.org/10.1016/J.ENERGY.2018.03.001.
[19] Chester - Compressed heat energy storage for energy from renewable sources: the project, n.d. https://www.chester-project.eu/. (Accessed 20 March 2023).
[20] A. White, G. Parks, C.N. Markides, Thermodynamic analysis of pumped thermal electricity storage, Appl. Therm. Eng. 53 (2013) 291–298, https://doi.org/10.1016/j.applthermaleng.2012.03.030.
[21] Y.M. Kim, D.G. Shin, S.Y. Lee, D. Favrat, Isothermal transcritical CO2 cycles with TES (thermal energy storage) for electricity storage, Energy 49 (2013) 484–501, https://doi.org/10.1016/j.energy.2012.09.057.
[22] J.D. McTigue, A.J. White, C.N. Markides, Parametric studies and optimisation of pumped thermal electricity storage, Appl. Energy 137 (2015) 800–811, https://doi.org/10.1016/j.apenergy.2014.08.039.
[23] W.D. Steinmann, The CHEST (Compressed Heat Energy STorage) concept for facility scale thermo mechanical energy storage, Energy 69 (2014) 543–552, https://doi.org/10.1016/j.energy.2014.03.049.
[24] S. Henchoz, F. Buchter, D. Favrat, M. Morandin, M. Mercangöz, Thermoeconomic analysis of a solar enhanced energy storage concept based on thermodynamic

cycles, Energy 45 (2012) 358–365, https://doi.org/10.1016/j.energy.2012.02.010.
[25] D. Fiaschi, G. Manfrida, K. Petela, L. Talluri, Thermo-electric energy storage with solar heat integration: exergy and exergo-economic analysis, Energies (Basel) 12 (2019), https://doi.org/10.3390/en12040648.
[26] P. Farres-Antunez, J. McTigue, A.J. White, A pumped thermal energy storage cycle with capacity for concentrated solar power integration, in: Offshore Energy and Storage Summit (OSES) (Brest, France), 2019.
[27] H. Jockenhöfer, W.D. Steinmann, D. Bauer, Detailed numerical investigation of a pumped thermal energy storage with low temperature heat integration, Energy 145 (2018) 665–676, https://doi.org/10.1016/j.energy.2017.12.087.
[28] M. Geyer, Decarbonization of coal fired power plants using high temperature thermal storage technologies from solar power plants, in: Int. Workshop on Carnot Batteries (Stuttgart, Germany), 2018.
[29] S. Schimpf, R. Span, Techno-economic evaluation of a solar assisted combined heat pump - organic Rankine cycle system, Energ. Conver. Manage. 94 (2015) 430–437, https://doi.org/10.1016/j.enconman.2015.02.011.
[30] O. Dumont, S. Quoilin, V. Lemort, Experimental investigation of a reversible heat pump/organic Rankine cycle unit designed to be coupled with a passive house to get a net zero energy building, Int. J. Refrig. 54 (2015) 190–203, https://doi.org/10.1016/j.ijrefrig.2015.03.008.
[31] S. Hu, Z. Yang, J. Li, Y. Duan, Thermo-economic analysis of the pumped thermal energy storage with thermal integration in different application scenarios, Energ. Conver. Manage. 236 (2021), 114072, https://doi.org/10.1016/J.ENCONMAN.2021.114072.
[32] D. Steger, C. Regensburger, B. Eppinger, S. Will, J. Karl, E. Schlücker, Design aspects of a reversible heat pump - organic rankine cycle pilot plant for energy storage, Energy 208 (2020), https://doi.org/10.1016/j.energy.2020.118216.
[33] CHESTER (Compressed Heat Energy STorage for Energy from Renewable sources) Project, D3.2 - Detailed Design of the High Temperature Heat Pump Laboratory Prototype. https://www.chester-project.eu/, 2019. (Accessed 5 July 2023).
[34] M.H. Nozari, M. Yaghoubi, K. Jafarpur, G.A. Mansoori, Development of dynamic energy storage hub concept: a comprehensive literature review of multi storage systems, J. Energy Storage 48 (2022), 103972, https://doi.org/10.1016/J.EST.2022.103972.
[35] L. Migliari, G. Cau, D. Cocco, V. Tola, A simplified approach for energy system design in buildings and its application to a case study, J. Phys. Conf. Ser. XXXX (2023) [Forthcoming].
[36] The MathWorks Inc, MATLAB Version: (R2023a) Update 3, n.d. https://www.mathworks.com, 2023. (Accessed 2 August 2023).
[37] Meteonorm, Meteonorm Features. Https://Meteonorm.Com/En/Meteonorm-Features, 2022.
[38] M. Petrollese, G. Concas, F. Lonis, D. Cocco, Techno-economic assessment of green hydrogen valley providing multiple end-users, Int. J. Hydrogen Energy 47 (2022), https://doi.org/10.1016/j.ijhydene.2022.04.210.
[39] J.A. Duffie, W.A. Beckman, W.M. Worek, Solar Engineering of Thermal Processes, in: J Sol Energy Eng, 2nd ed., 116, 1994, https://doi.org/10.1115/1.2930068.
[40] SunPower®, SunPower® X-Series Solar Panels | X22-360, n.d. https://sunpower.maxeon.com/it/sites/default/files/2019-09/sunpower-maxeon-serie-x-x22-360-x21-345-commerciale.pdf. (Accessed 19 September 2023).
[41] Enogia, ORC ENO-10LT Datasheet. www.enogia.com, 2023.
[42] M.E. Mondéjar, M.O. Mclinden, E.W. Lemmon, Thermodynamic properties of trans-1-chloro-3,3,3-trifluoropropene (R1233zd(E)): vapor pressure, (p, ρ, T) behavior, and speed of sound measurements, and equation of state, J. Chem. Eng. Data 60 (2015) 2477–2489, https://doi.org/10.1021/ACS.JCED.5B00348/SUPPL_FILE/JE5B00348_SI_001.PDF.
[43] L.X. Chen, P. Hu, P.P. Zhao, M.N. Xie, F.X. Wang, Thermodynamic analysis of a High Temperature Pumped Thermal Electricity Storage (HT-PTES) integrated with a parallel organic Rankine cycle (ORC), Energ. Conver. Manage. 177 (2018) 150–160, https://doi.org/10.1016/J.ENCONMAN.2018.09.049.
[44] S. Dong, X. Hu, J.F. Huang, T. Zhu, Y. Zhang, X. Li, Investigation on improvement potential of ORC system off-design performance by expander speed regulation based on theoretical and experimental exergy-energy analyses, Energy 220 (2021), 119753, https://doi.org/10.1016/J.ENERGY.2021.119753.
[45] M. Weitzer, D. Müller, J. Karl, Two-phase expansion processes in heat pump – ORC systems (Carnot batteries) with volumetric machines for enhanced off-design efficiency, Renew Energy 199 (2022) 720–732, https://doi.org/10.1016/J.RENENE.2022.08.143.
[46] F. Fatigati, D. Vittorini, M. Di Bartolomeo, R. Cipollone, Experimental characterization of a small-scale solar Organic Rankine Cycle (ORC) based unit for domestic microcogeneration, Energ. Conver. Manage. 258 (2022), 115493, https://doi.org/10.1016/J.ENCONMAN.2022.115493.
[47] J. Raccanello, S. Rech, A. Lazzaretto, Simplified dynamic modeling of single-tank thermal energy storage systems, Energy 182 (2019) 1154–1172, https://doi.org/10.1016/J.ENERGY.2019.06.088.
[48] UNI EN 14825:2022, (n.d.).
[49] Q. Iqbal, S. Fang, Y. Zhao, Y. Yao, Z. Xu, H. Gan, H. Zhang, L. Qiu, C.N. Markides, K. Wang, Thermo-economic assessment of sub-ambient temperature pumped-thermal electricity storage integrated with external heat sources, Energ. Conver. Manage. 285 (2023), 116987, https://doi.org/10.1016/J.ENCONMAN.2023.116987.
[50] V. Jülch, Comparison of electricity storage options using levelized cost of storage (LCOS) method, Appl. Energy 183 (2016) 1594–1606, https://doi.org/10.1016/J.APENERGY.2016.08.165.
[51] A. Smallbone, V. Jülch, R. Wardle, A.P. Roskilly, Levelised cost of storage for pumped heat energy storage in comparison with other energy storage technologies, Energ. Conver. Manage. 152 (2017) 221–228, https://doi.org/10.1016/J.ENCONMAN.2017.09.047.
[52] D.S. Ayou, V. Eveloy, Energy, exergy and exergoeconomic analysis of an ultra low-grade heat-driven ammonia-water combined absorption power-cooling cycle for district space cooling, sub-zero refrigeration, power and LNG regasification, Energ. Conver. Manage. 213 (2020), 112790, https://doi.org/10.1016/J.ENCONMAN.2020.112790.
[53] IEA SHC Task52 - Deliverable C1: Classification and benchmarking of solar thermal systems in urban environments, n.d. https://www.researchgate.net/publication/329060076_IEA_SHC_Task52_-_Deliverable_C1_Classification_and_benchmarking_of_solar_thermal_systems_in_urban_environments?channel=doi&linkId=5bf3e5db92851c6b27cc2e0a&showFulltext=true. (Accessed 17 November 2023).
[54] C. Roselli, G. Diglio, M. Sasso, F. Tariello, A novel energy index to assess the impact of a solar PV-based ground source heat pump on the power grid, Renew. Energy 143 (2019) 488–500, https://doi.org/10.1016/J.RENENE.2019.05.023.